Featured in Physics

Mott Transition for a Lieb-Liniger Gas in a Shallow Quasiperiodic Potential: Delocalization Induced by Disorder

Hepeng Yao,[1,*] Luca Tanzi,[2,3] Laurent Sanchez-Palencia,[4] Thierry Giamarchi,[1] Giovanni Modugno,[2,3,5] and Chiara D'Errico[6,†]

[1]DQMP, University of Geneva, 24 Quai Ernest-Ansermet, CH-1211 Geneva, Switzerland
[2]Istituto Nazionale di Ottica, CNR-INO, Via Moruzzi 1, 56124 Pisa, Italy
[3]European Laboratory for Non-Linear Spectroscopy, Università degli Studi di Firenze, Via N. Carrara 1, 50019 Sesto Fiorentino, Italy
[4]CPHT, CNRS, Ecole Polytechnique, IP Paris, F-91128 Palaiseau, France
[5]Dipartimento di Fisica e Astronomia, Università degli Studi di Firenze, Via G. Sansone 1, 50019 Sesto Fiorentino, Italy
[6]Istituto per la Protezione Sostenibile delle Piante, CNR-IPSP, Strada delle Cacce 73, 10135 Torino, Italy

(Received 23 February 2024; accepted 9 July 2024; published 19 September 2024)

Disorder or quasidisorder is known to favor localization in many-body Bose systems. Here, in contrast, we demonstrate an anomalous delocalization effect induced by incommensurability in quasiperiodic lattices. Loading ultracold atoms in two shallow periodic lattices with equal amplitude and either equal or incommensurate spatial periods, we show the onset of a Mott transition not only in the periodic case but also in the quasiperiodic case. Switching from periodic to quasiperiodic potential with the same amplitude, we find that the Mott insulator turns into a delocalized superfluid. Our experimental results agree with quantum Monte Carlo calculations, showing this anomalous delocalization induced by the interplay between the disorder and interaction.

DOI: 10.1103/PhysRevLett.133.123401

The Mott insulator (MI) is one of the most remarkable paradigmatic phases in strongly correlated quantum materials [1–3]. It appears in condensed-matter systems when correlation effects associated with the strong electron-electron repulsion drive a metal-insulator phase transition [4]. The MI characterizes a broad class of materials [5–10], and is related to exotic quantum phenomena such as high critical temperature superconductivity [11], fractional quantum Hall effect [12,13], and topological phase transitions [14]. MIs also appear in bosonic lattice models due to the competition between tunneling and repulsive interactions [15]. Experiments with ultracold atoms in optical lattices allow for in-depth investigation of many-body physics in a broad range of models [16–19] and are proved instrumental for direct observation and characterization of Mott phases for both Bose [15,20,21] and Fermi [22,23] systems, first in three dimensions and later also in lower dimensional systems [24–30]. Remarkably, for one-dimensional (1D) bosonic systems with sufficiently strong repulsive interactions, a purely periodic potential with arbitrary small amplitude can stabilize a Mott phase [31–35], as confirmed experimentally in Refs. [36,37].

Recently, quasiperiodic systems realized by two periodic lattices with incommensurate spatial periods have attracted a lot of attention. Disorder induced by such quasiperiodic potentials induces intriguing quantum phenomena such as Anderson localization [38–40], Bose glass (BG) [41–43], and fractional MIs [44,45]. The phase diagrams of interacting bosons in such systems have been extensively studied theoretically both in one [44–46] and two [47,48] dimensions and recent experiments have reported measurements for 1D tight-binding models [40,49,50] and 2D quasicrystals [51,52].

Quasiperiodic lattices offer the possibility of studying the open problem of localization versus delocalization in the presence of disorder induced by incommensurate potentials. Bosons in a 1D periodic lattice with incommensurate filling always exhibit an extended superfluid (SF) phase at zero temperature. Changing from a periodic to a quasiperiodic lattice, although keeping the total amplitude unchanged, the system will tend to localize and form a BG phase, as illustrated in the first row of Fig. 1(a). This suggests that quasiperiodicity favors localization. However, when the number of particles is commensurate with the total number of the lattice sites, the situation is completely opposite. As illustrated in the second row of Fig. 1(a), while the periodic case favors a localized MI phase, the quasiperiodic case will favor the delocalized superfluid phase. While the Mott transition in periodic system has been assessed [36,37], the quasiperiodic case, especially the delocalizing effect induced by incommensurability, is still a conjecture.

In this work, we experimentally observe the interplay of disorder and interaction in a strongly correlated Bose gas

*Contact author: Hepeng.Yao@unige.ch
†Contact author: chiara.derrico@cnr.it

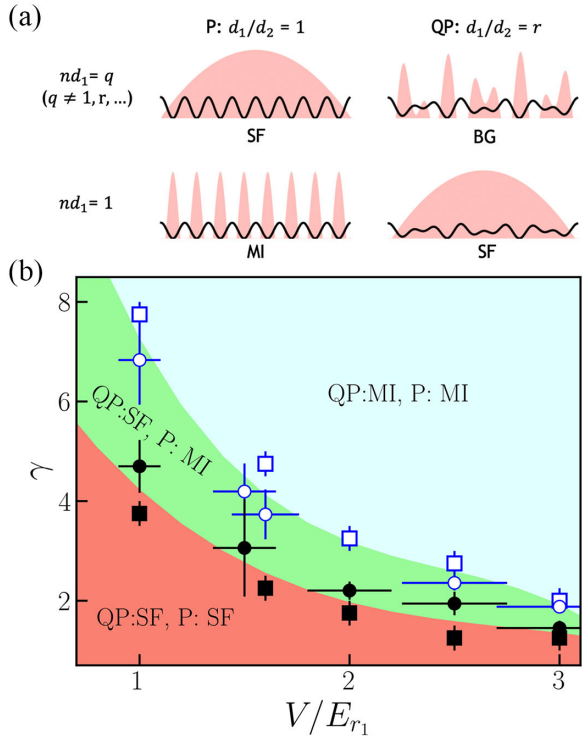

FIG. 1. Quantum phase transitions in periodic (P) and quasiperiodic (QP) systems. (a) Sketch of a strongly interacting Bose gas for different commensurability: $nd_1 = q$ ($q \neq 1, r, 1-r\ldots$, top) and $nd_1 = 1$ (bottom), for periodic (left) and quasiperiodic (right) systems with d_1 the lattice period with larger spacing. (b) Phase diagram for the MI-to-SF transition versus interaction strength and potential amplitude for unit particle filling $nd_1 = 1$. The transition lines are drawn as cubic polynomial fits of both experimental (disk and circles) and QMC (squares) data points, for both periodic (solid markers) and quasiperiodic (hollow markers) systems.

using ultracold atoms in an optical lattice with switchable commensurability. We use two shallow periodic lattices with equal amplitude and either equal or incommensurate spatial periods. Using transport and excitation measurements, we show the onset of a Mott transition in the quasiperiodic case, at a different lattice amplitude than the one already observed in the periodic case [36,37]. The experiment is in good agreement with quantum Monte Carlo (QMC) calculations. Comparing the phase diagrams in the periodic and quasiperiodic cases, both theory and experiment show anomalous delocalization arising from disorder.

System and quantum phase diagram—We consider a low temperature 1D gas of interacting bosons (Lieb-Liniger gas) in the presence of an external lattice potential. Its Hamiltonian writes

$$\mathcal{H} = \sum_{1\leq j\leq N}\left[-\frac{\hbar^2}{2m}\frac{\partial^2}{\partial z_j^2} + V(z_j)\right] + g_{1D}\sum_{j<\ell}\delta(z_j - z_\ell), \quad (1)$$

with m the atomic mass, z_j the position of particle j, and $g_{1D} = -2\hbar^2/ma_{1D}$ the coupling constant, with a_{1D} the 1D scattering length. In the experiment, 1D tubes are created by strong transverse confinement, and a_{1D} is related to the 3D scattering length a and to the transverse oscillator length $\ell_\perp = \sqrt{\hbar/m\omega_\perp}$ via $a_{1D} = \ell_\perp^2(1 - 1.03a/\ell_\perp)/a$ [53,54]. The quasiperiodic potential writes

$$V(z) = \frac{V}{2}[\sin^2(k_1 z) + \sin^2(k_2 z + \varphi)], \quad (2)$$

with V the potential amplitude, $k_i = \pi/d_i (i = 1, 2)$ the lattice wave vectors, and d_i the lattice periods. The recoil energy of each lattice is $E_{ri} = \hbar^2 k_i^2/2m$. By controlling the ratio between the two wave vectors, we can realize either a periodic ($k_1 = k_2$, $\varphi = 0$) or quasiperiodic ($k_2/k_1 = r$ with r irrational, arbitrary φ) lattice. Here we use $r \simeq 1.2386\ldots$. In the experiment, the interaction strength, measured in terms of the Lieb-Liniger parameter $\gamma = mg_{1D}/\hbar^2 n$, is controlled using Feshbach resonance techniques.

Figure 1(b) summarizes our main results: it shows the quantum phase diagram of the Lieb-Liniger gas in the presence of either a pure periodic or quasiperiodic potential with same global amplitude $\max[V(x)] - \min[V(x)]$, at particle filling $nd_1 = 1$ ($nd_2 = 1/r < 1$). The two axes indicate the total potential amplitude V and the Lieb-Liniger parameter γ. We focus on the shallow lattice case where $V \sim E_{r1}$. In principle, theory predicts the existence of three different phases: the SF, the gapped MI, and the gapless BG. Nevertheless, a sizable BG phase should appear only for potential depth V larger than the critical value $V_c \approx 4.2E_{r1}$ [45,55], which is beyond our measured regime. Hence, only MI and SF appear in the phase diagram. Here, we show the MI-SF transition points from both experiment of phase-slip-induced dissipation measurement (circles) and QMC calculations of superfluid fraction (squares). More details about these techniques are presented in the later sections.

For weak interaction and small lattice amplitude, both the periodic and quasiperiodic systems are superfluid (red region, SF). For strong interaction and larger lattice amplitude, we find that both stabilize an MI with unit filling with respect to the first lattice (blue region). These two domains are separated by a genuine phase transition, but the critical interaction strength γ_c differs in the periodic and quasiperiodic cases. The green region shows the domain where the periodic potential stabilizes an MI phase while the quasiperiodic potential induces an SF phase. For the periodic case, the experimental data for the Mott transition (black disks) is the one of Ref. [37]. The demonstration of the Mott transition in the quasiperiodic case, i.e., the second transition line (corresponding to the open blue markers) between the green and blue regions is the first main result of our work. It is the first experimental demonstration of the Mott transition in a non-purely-periodic atomic

system. The second main result is the existence of the green region where the system is an MI phase in the periodic case and quasiperiodicity restores a stable SF phase, hence emphasizing the crucial role of commensurability versus incommensurability. This confirms the conjectured picture suggested in Fig. 1(a): it indicates that the quasiperiodic lattice favors delocalization and induces an SF phase when the particle filling is commensurate with one of the lattice periods. Contrary to common situations where disorder leads to localization, the existence of the green area here suggests an anomalous delocalization effect induced by disorder. This is due to the fact that the presence of the second lattice blurs the periodicity of the first one, which is commensurate with the particle filling, since $nd_1 = 1$ but $nd_2 < 1$.

Experimental measurement of the transition—The experiment starts with a Bose-Einstein condensate (BEC) with about 35×10^3 atoms of ^{39}K with tunable scattering length [56]. It is then loaded into a strong 2D horizontal optical lattice, which splits the sample into about 1500 vertical tubes with a radial trapping frequency $\omega_\perp = 2\pi \times 40$ kHz. Each tube contains on average 33 atoms and has a longitudinal harmonic trap potential with frequency $\omega_z = 2\pi \times$ 160 Hz. Both intertubes and intratubes, the atom distribution is inhomogeneous. The mean density $\bar{n}$ is then calculated by averaging over all the tubes [40,57]. Note our 3D BEC is prepared at a temperature presumably lower than 10 nK. Suggested by recent works [60–62], a further cooling may appear during the dimensional reduction.

For the incommensurate case, we then adiabatically raise two weak vertical optical lattices with the same amplitude $(V/2)$ and different wavelengths $\lambda_1 = 1064$ nm and $\lambda_2 = 859$ nm to transfer the system in the shallow potential of Eq. (2) with $k_i = 2\pi/\lambda_i$. For the commensurate case, we set $\lambda_2 = \lambda_1$. We use $a_{\text{load}} = 226a_0$ (a_0 is the Bohr radius) to obtain a mean density $\bar{n} = (0.99 \pm 0.12)/d_1 = (0.80 \pm 0.09)/d_2$. At this point we tune the scattering length to a variable value a (hence varying γ) and explore the transport properties of the system in the $\gamma - V$ diagram.

By suddenly switching off a levitating vertical magnetic field gradient, we shift the center of the harmonic trap by $\delta z \approx 3$ μm and excite a sloshing motion of the system in the longitudinal (vertical) direction. After a variable evolution time t, we switch off all external confinements and let the atoms free to expand for $t_{\text{TOF}} = 16.5$ ms before absorption images are recorded in time of flight (TOF). A typical image is shown in Fig. 2(a). By integrating along the radial direction we obtain the longitudinal atom distributions, whose peak position z can be detected at different evolution time t [Fig. 2(b)].

In Fig. 2(b) we show an example of the evolution of the atomic density peak position z for fixed values of both the quasiperiodic potential depth V and the scattering length a (cyan circles). Typically we observe an initial increase of the peak position z up to a certain critical value z_c, followed by a decrease for larger times. This behavior is expected for

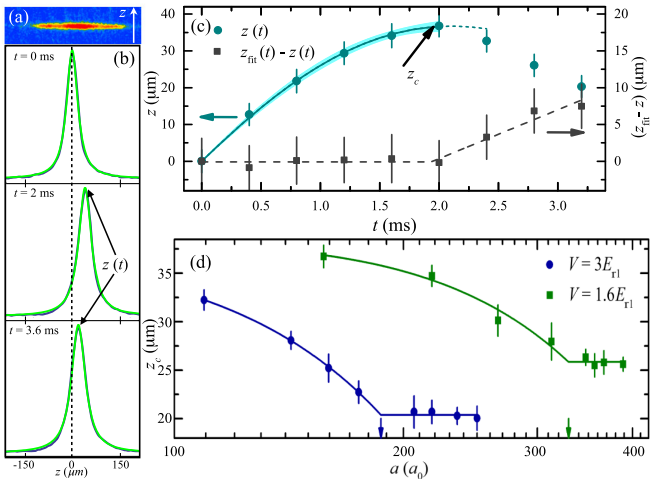

FIG. 2. (a) A representative absorption image of atoms in time of flight (TOF). (b) Three representative atom distributions along the longitudinal direction at different evolution time t. (c) Evolution of the atomic peak position z for a quasiperiodic potential with $V = (1.60 \pm 0.16)E_{\text{r1}}$ and $a = (157 \pm 2)a_0$ (cyan circles, left-hand axis) and difference between the fit of the evolution for $z < z_c$ (z_{fit}) and the experimental data (gray squares, right-hand axis). The error bars are the squared sum of a standard deviation of 4–6 independent measurements and the imaging resolution. The solid cyan (dashed gray) line is a damped oscillation (piecewise) fit to the experimental data at short (at any) time. The shaded area shows the 95% confidence band of the oscillation fit. (d) Critical value z_c versus a for two values of the potential depth: $V = (3.0 \pm 0.3)E_{\text{r1}}$ (blue circles) and $V = (1.60 \pm 0.16)E_{\text{r1}}$ (green squares). The error bars come from the fit used to extract z_c and represent the statistical uncertainties. Solid lines are the piecewise fit to extract the critical value of the SF-MI critical point a_c (arrows) and its uncertainty: $a_c = (187 \pm 2)a_0$ and $a_c = (330 \pm 15)a_0$, respectively, for $V = 3E_{\text{r1}}$ and $V = 1.6E_{\text{r1}}$.

a 1D system, in which the presence of phase-slip events typically induces dissipation in its dynamics [63–65]. The data for $z < z_c$ are fitted by a damped oscillation $z_{\text{fit}}(t) = z_{\max} e^{-Gt} \sin(\omega' t)$, with $\omega' = \sqrt{\omega^{*2} - 4\pi^2 G^2}$, $\omega^* = \omega_z \sqrt{m/m^*}$, m^* the effective mass in the quasiperiodic potential, and $z_{\max} = (m^* \omega^{*2} \delta z t_{\text{TOF}}/m\omega')$. G and δz are fitting parameters. For larger times, the system enters a strongly dissipative regime where the phase-slip nucleation rate diverges [64,66]. By fitting the difference between the damped oscillation $z_{\text{fit}}(t)$ and the experimental data at any time with a piecewise function (gray squares), we extract the critical value z_c and its uncertainty. In the presence of a single periodic potential, the critical value z_c is known to decrease with increasing interactions in both deep [36,66] and shallow [37,64] optical lattices, and to vanish (reach a constant value) at the SF-MI transition in the former (latter) regime. We observe a similar behavior with the quasiperiodic lattice. In Fig. 2(d) we show the value z_c for increasing scattering length a for two values of the quasiperiodic

potential depth V. As already observed for a single weak lattice potential [37], z_c decreases for increasing a and reaches a plateau for $a > a_c$. The quantity a_c can then be interpreted as the critical scattering length to enter the Mott lobe associated to the largest density $(1/d_1)$. We use a piecewise function with a second-order polynomial fit to extract a_c and its uncertainty. Consistently with theoretical predictions, we find that a_c increases as V decreases.

In Fig. 1(b) we show the critical interaction strength, expressed in terms of γ, for the superfluid-insulator transitions measured for several values of the potential depth V, in both periodic (black disks) and quasiperiodic (blue circles) cases. In both cases, we find that γ_c monotonically decreases with V, but the critical value to enter the MI regime is significantly higher for the quasiperiodic case than for the periodic case, as discussed above.

Quantum Monte Carlo calculations—We now discuss the numerical calculations. Using continuous-space path integral quantum Monte Carlo calculations [67] with the worm algorithm implementation [68,69], we simulate strongly interacting 1D bosons in the presence of a shallow potential, be it periodic or quasiperiodic. For given values of the chemical potential μ, the temperature T, and the interaction strength g_{1D}, we compute the particle density n and superfluid fraction f_s. The SF phase is characterized by $f_s > 0$, whereas the MI phase corresponds to $f_s = 0$ and a plateau at $nd_1 = 1$. We use the system size $L = 100d_1$ and temperature $T \sim 3$ nK. In practice, we judge the MI phase using the criteria $f_s < 5\%$ and $|1 - nd_1| < 5\%$ [37]. Note that we do not observe any cases where $f_s \simeq 0$ and $nd_1 \neq 1$, consistent with the absence of a BG phase in the considered parameter range.

In Fig. 3, we show the phase diagram versus inverse interaction strength $1/\gamma$ and chemical potential μ for the quasiperiodic case with $V = 3E_{r1}$. We find an MI lobe with $nd_1 = 1$ (blue) surrounded by the SF phase (red). The SF-MI transitions are shown as black squares. At the tip of the Mott lobe, we use the resolution $\delta\mu = 0.01E_{r1}$ (such that $\delta\mu < k_B T$) and $\delta g_{1D} = 0.5\hbar^2/m$. This allows us to locate the critical value of γ accurately. In this given example, we find $\gamma_c = 2.0 \pm 0.25$ (blue cross) [57].

With this procedure, we compute the critical interaction strength γ_c as a function of the potential amplitude V, for both periodic $(k_1 = k_2, \varphi = 0)$ and quasiperiodic $(k_1 \neq k_2, \varphi = 0.2)$ shallow potentials; see Eq. (2). The final data are shown as solid black (quasiperiodic) and hollow blue (periodic) squares in Fig. 1(b). We find that theory and experiment agree within error bars. This further confirms the existence of a region (green) where the periodic system enters the MI phase, but quasiperiodicity restores a stable SF. The small deviation between theory and experiment may originate from the finite temperature and inhomogeneity effects in the experiment and the finite resolution $\delta\mu$ in the numerics. Note that here we observe a direct SF-MI transition up to our resolution. Although no sizable BG is presented, whether there exists a tiny BG sliver in between is an open question that deserves further analysis [42,43,70].

Detection of the Mott gap—The MI phase is further characterized by the emergence of a finite gap in the excitation spectrum. In the experiment, we modulate the depth of the quasiperiodic potential as $V(t) = V[1 + A\cos(2\pi\nu t)]$, with $A \simeq 0.1$ for 200 ms so as to generate excitations at the frequency ν [40]. We then transfer back the Bose gas into the 3D optical trap by switching off all lattice beams and measure the variation of the BEC fraction as a function of the modulation frequency ν [71,72]. Figure 4 shows two characteristic results respectively below and above the

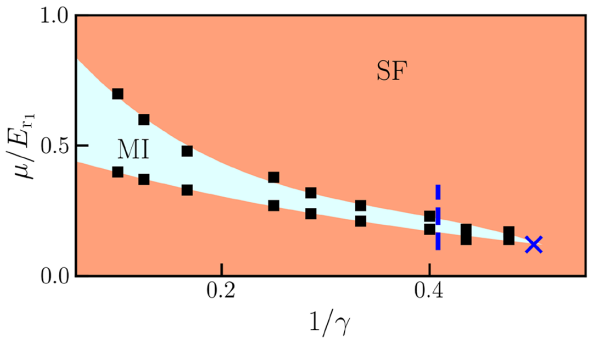

FIG. 3. Phase diagram versus the inverse interaction parameter $1/\gamma$ and chemical potential μ for the quasiperiodic case with amplitude $V = 3E_{r1}$, computed using QMC calculations. The system size is $L = 100d_1$ and the temperature $T \sim 3$ nK. The MI lobe (blue), the SF region (red), and the critical point γ_c (blue cross) are determined from the SF-MI transition points (black squares). The dashed blue line indicates the coupling constant $\widetilde{g_{1D}} = 2.46$ where the excitation gap is studied; see Fig. 4.

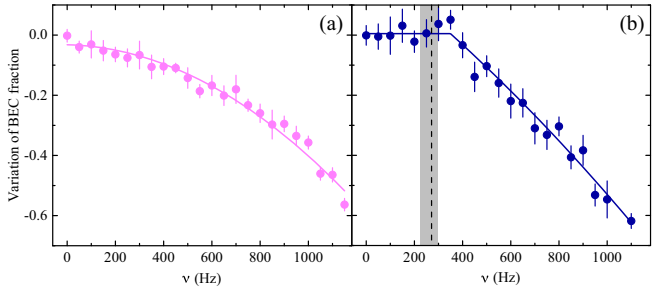

FIG. 4. Excitation spectra for a quasiperiodic lattice with depth $V = 3E_{r1}$ and two different scattering lengths (a) below and (b) above the critical value a_c for the fluid-insulator transition: $a = (142.4 \pm 1.9)a_0$ and $a = (235 \pm 5)a_0$, respectively. The error bars are a standard deviation of about 8 independent measurements. Solid lines are fits with a second-order polynomial piecewise function. The vertical dashed line corresponds to the theoretical prediction for $a = 235a_0$ and $T = 3$ nK, while the gray area indicates its uncertainty, resulting from the systematic error on a and $\ell_\perp$ in the experiment and the error bar from QMC calculations [57].

localization transition. As expected, for weak interactions, any small modulation frequency is able to excite the system, corresponding to a gapless SF phase [Fig. 4(a)]. In contrast, for strong interactions, no excitation is observed up to some frequency gap, corresponding to the MI phase [Fig. 4(b)]. For $V = 3E_{r1}$, the measured gap is $\nu_g = (350 \pm 50)$ Hz and is consistent, within error bars, with the Mott gap calculated in the QMC simulations for the same parameters as in the experiment and low T [see dashed blue vertical line in Fig. 3 and dashed black line in Fig. 4(b)]. This further corroborates that the observed insulating phase is a gapped MI with density $n = 1/d_1$, instead of a gapless BG.

Discussion—We have demonstrated the onset of a Mott transition in a shallow 1D quasiperiodic lattice. In the range $1 < V/E_{r1} < 3$ and for $\overline{n} = 1/d_1$, the critical value of the interaction strength is larger in the quasiperiodic case compared to the periodic case. It shows that in this regime disorder due to the quasiperiodic potential stabilizes the SF phase, i.e., an anomalous disorder-induced delocalization. This may be qualitatively understood within renormalization group analysis similarly as in Refs. [35–37,70]: for $nd_1 = 1$, only the first lattice is relevant while the second lattice is irrelevant, within first-order approximation, hence lowering the effective strength of the pinning potential. Still, the SF-to-MI transition observed in the incommensurate case is not quantitatively similar to that for a single lattice, which implies significant renormalization of the effective strength of the first lattice by the second. This mechanism may prefigure the onset of a BG phase for stronger potential amplitudes.

Our work provides an essential contribution to understanding the pivotal role played by disorder and commensurability in quantum phase transitions. Moreover, further experimental control would allow us to investigate more complex quantum phases, such as fractional MIs and BG phases [45,47,48,55].

Acknowledgments—This research was supported by the QuantERA Programme that has received funding from the European Union's Horizon 2020 research and innovation programme under Grant Agreements No. 731473 and No. 101017733, project MAQS, with funding organization Consiglio Nazionale delle Ricerche, by the Agence Nationale de la Recherche (ANR, Project No. ANR-CMAQ-002 France 2030), the program "Investissements d'Avenir" LabEx PALM (Project No. ANR-10-LABX-0039-PALM), the Swiss National Science Foundation under Grants No. 200020-188687 and No. 200020-219400. H. Y., L. S.-P., and T. G. thank the Institut Henri Poincaré (UAR 839 CNRS-Sorbonne Université) and the LabEx CARMIN (ANR-10-LABX-59-01) for their support. Numerical calculations make use of the ALPS scheduler library and statistical analysis tools [73–75].

[1] N. F. Mott and R. Peierls, Discussion of the paper by de Boer and Verwey, Proc. Phys. Soc. London **49**, 72 (1937).
[2] N. Mott, The basis of the electron theory of metals, with special reference to the transition metals, Proc. R. Soc. A **62**, 416 (1949).
[3] N. F. Mott, On the transition to metallic conduction in semiconductors, Can. J. Phys. **34**, 1356 (1956).
[4] M. Imada, A. Fujimori, and Y. Tokura, Metal-insulator transitions, Rev. Mod. Phys. **70**, 1039 (1998).
[5] P. A. Lee, N. Nagaosa, and X.-G. Wen, Doping a Mott insulator: Physics of high-temperature superconductivity, Rev. Mod. Phys. **78**, 17 (2006).
[6] T. Furukawa, K. Miyagawa, H. Taniguchi, R. Kato, and K. Kanoda, Quantum criticality of Mott transition in organic materials, Nat. Phys. **11**, 221 (2015).
[7] Y. Cao, V. Fatemi, A. Demir, S. Fang, S. L. Tomarken, J. Y. Luo, J. D. Sanchez-Yamagishi, K. Watanabe, T. Taniguchi, E. Kaxiras *et al.*, Correlated insulator behaviour at half-filling in magic-angle graphene superlattices, Nature (London) **556**, 80 (2018).
[8] Y. Tang, L. Li, T. Li, Y. Xu, S. Liu, K. Barmak, K. Watanabe, T. Taniguchi, A. H. MacDonald, J. Shan *et al.*, Simulation of Hubbard model physics in WSe_2/WS_2 moiré superlattices, Nature (London) **579**, 353 (2020).
[9] E. C. Regan, D. Wang, C. Jin, M. I. Bakti Utama, B. Gao, X. Wei, S. Zhao, W. Zhao, Z. Zhang, K. Yumigeta *et al.*, Mott and generalized Wigner crystal states in WSe_2/WS_2 moiré superlattices, Nature (London) **579**, 359 (2020).
[10] Y. Shimazaki, I. Schwartz, K. Watanabe, T. Taniguchi, M. Kroner, and A. Imamoğlu, Strongly correlated electrons and hybrid excitons in a moiré heterostructure, Nature (London) **580**, 472 (2020).
[11] E. Dagotto, Correlated electrons in high-temperature superconductors, Rev. Mod. Phys. **66**, 763 (1994).
[12] A. A. Burkov, Fractional quantum Hall effect and featureless Mott insulators, Phys. Rev. B **81**, 125111 (2010).
[13] Y. Kuno, K. Shimizu, and I. Ichinose, Bosonic analogs of the fractional quantum Hall state in the vicinity of Mott states, Phys. Rev. A **95**, 013607 (2017).
[14] S. Sen, P. J. Wong, and A. K. Mitchell, The Mott transition as a topological phase transition, Phys. Rev. B **102**, 081110 (R) (2020).
[15] M. Greiner, O. Mandel, T. Esslinger, T. W. Hänsch, and I. Bloch, Quantum phase transition from a superfluid to a Mott insulator in a gas of ultracold atoms, Nature (London) **415**, 39 (2002).
[16] I. Bloch, J. Dalibard, and W. Zwerger, Many-body physics with ultracold gases, Rev. Mod. Phys. **80**, 885 (2008).
[17] L. Tarruell and L. Sanchez-Palencia, Quantum simulation of the Hubbard model with ultracold fermions in optical lattices, C.R. Phys. **19**, 365 (2018).
[18] T. Esslinger, Fermi-Hubbard physics with atoms in an optical lattice, Annu. Rev. Condens. Mater. Phys. **1**, 129 (2010).
[19] C. Gross and I. Bloch, Quantum simulations with ultracold atoms in optical lattices, Science **357**, 995 (2017).
[20] F. Gerbier, A. Widera, S. Fölling, O. Mandel, T. Gericke, and I. Bloch, Phase coherence of an atomic Mott insulator, Phys. Rev. Lett. **95**, 050404 (2005).

[21] F. Gerbier, A. Widera, S. Fölling, O. Mandel, T. Gericke, and I. Bloch, Interference pattern and visibility of a Mott insulator, Phys. Rev. A **72**, 053606 (2005).
[22] R. Jördens, N. Strohmaier, K. Günter, H. Moritz, and T. Esslinger, A Mott insulator of fermionic atoms in an optical lattice, Nature (London) **455**, 204 (2008).
[23] U. Schneider, L. Hackermüller, S. Will, T. Best, I. Bloch, T. A. Costi, R. W. Helmes, D. Rasch, and A. Rosch, Metallic and insulating phases of repulsively interacting fermions in a 3D optical lattice, Science **322**, 1520 (2008).
[24] T. Stöferle, H. Moritz, C. Schori, M. Köhl, and T. Esslinger, Transition from a strongly interacting 1D superfluid to a Mott insulator, Phys. Rev. Lett. **92**, 130403 (2004).
[25] I. B. Spielman, W. D. Phillips, and J. V. Porto, Mott-insulator transition in a two-dimensional atomic Bose gas, Phys. Rev. Lett. **98**, 080404 (2007).
[26] I. B. Spielman, W. D. Phillips, and J. V. Porto, Condensate fraction in a 2D Bose gas measured across the Mott-insulator transition, Phys. Rev. Lett. **100**, 120402 (2008).
[27] D. Greif, T. Uehlinger, G. Jotzu, L. Tarruell, and T. Esslinger, Short-range quantum magnetism of ultracold fermions in an optical lattice, Science **340**, 1307 (2013).
[28] D. Greif, G. Jotzu, M. Messer, R. Desbuquois, and T. Esslinger, Formation and dynamics of antiferromagnetic correlations in tunable optical lattices, Phys. Rev. Lett. **115**, 260401 (2015).
[29] E. Cocchi, L. A. Miller, J. H. Drewes, M. Koschorreck, D. Pertot, F. Brennecke, and M. Köhl, Equation of state of the two-dimensional Hubbard model, Phys. Rev. Lett. **116**, 175301 (2016).
[30] J. H. Drewes, E. Cocchi, L. A. Miller, C. F. Chan, D. Pertot, F. Brennecke, and M. Köhl, Thermodynamics versus local density fluctuations in the metal–Mott-insulator crossover, Phys. Rev. Lett. **117**, 135301 (2016).
[31] F. D. M. Haldane, Solidification in a soluble model of bosons on a one-dimensional lattice: The Boson-Hubbard chain, J. Phys. Lett. A **80**, 281 (1980).
[32] F. D. M. Haldane, Effective harmonic-fluid approach to low-energy properties of one-dimensional quantum fluids, Phys. Rev. Lett. **47**, 1840 (1981).
[33] T. Giamarchi, Mott transition in one dimension, Physica (Amsterdam) **230–232B**, 975 (1997).
[34] T. Giamarchi, *Quantum Physics in One Dimension*, International Series of Monographs on Physics, Vol. 121 (Oxford University Press, Oxford, 2004).
[35] H.-P. Büchler, G. Blatter, and W. Zwerger, Commensurate-incommensurate transition of cold atoms in an optical lattice, Phys. Rev. Lett. **90**, 130401 (2003).
[36] E. Haller, R. Hart, M. J. Mark, J. G. Danzl, L. Reichsöllner, M. Gustavsson, M. Dalmonte, G. Pupillo, and H.-C. Nägerl, Pinning quantum phase transition for a Luttinger liquid of strongly interacting bosons, Nature (London) **466**, 597 (2010).
[37] G. Boéris, L. Gori, M. D. Hoogerland, A. Kumar, E. Lucioni, L. Tanzi, M. Inguscio, T. Giamarchi, C. D'Errico, G. Carleo *et al.*, Mott transition for strongly interacting one-dimensional bosons in a shallow periodic potential, Phys. Rev. A **93**, 011601(R) (2016).
[38] S. Aubry and G. André, Analyticity breaking and Anderson localization in incommensurate lattices, Ann. Isr. Phys. Soc. **3**, 133 (1980).
[39] L. Fallani, J. E. Lye, V. Guarrera, C. Fort, and M. Inguscio, Ultracold atoms in a disordered crystal of light: Towards a Bose glass, Phys. Rev. Lett. **98**, 130404 (2007).
[40] C. D'Errico, E. Lucioni, L. Tanzi, L. Gori, G. Roux, I. P. McCulloch, T. Giamarchi, M. Inguscio, and G. Modugno, Observation of a disordered bosonic insulator from weak to strong interactions, Phys. Rev. Lett. **113**, 095301 (2014).
[41] T. Giamarchi and H. J. Schulz, Localization and interactions in one-dimensional quantum fluids, Europhys. Lett. **3**, 1287 (1987).
[42] T. Giamarchi and H. J. Schulz, Anderson localization and interactions in one-dimensional metals, Phys. Rev. B **37**, 325 (1988).
[43] M. P. A. Fisher, P. B. Weichman, G. Grinstein, and D. S. Fisher, Boson localization and the superfluid-insulator transition, Phys. Rev. B **40**, 546 (1989).
[44] G. Roux, T. Barthel, I. P. McCulloch, C. Kollath, U. Schollwöck, and T. Giamarchi, Quasiperiodic Bose-Hubbard model and localization in one-dimensional cold atomic gases, Phys. Rev. A **78**, 023628 (2008).
[45] H. Yao, T. Giamarchi, and L. Sanchez-Palencia, Lieb-Liniger bosons in a shallow quasiperiodic potential: Bose glass phase and fractal Mott lobes, Phys. Rev. Lett. **125**, 060401 (2020).
[46] T. Roscilde, Bosons in one-dimensional incommensurate superlattices, Phys. Rev. A **77**, 063605 (2008).
[47] R. Gautier, H. Yao, and L. Sanchez-Palencia, Strongly interacting bosons in a two-dimensional quasicrystal lattice, Phys. Rev. Lett. **126**, 110401 (2021).
[48] Z. Zhu, H. Yao, and L. Sanchez-Palencia, Thermodynamic phase diagram of two-dimensional bosons in a quasicrystal potential, Phys. Rev. Lett. **130**, 220402 (2023).
[49] L. Gori, T. Barthel, A. Kumar, E. Lucioni, L. Tanzi, M. Inguscio, G. Modugno, T. Giamarchi, C. D'Errico, and G. Roux, Finite-temperature effects on interacting bosonic one-dimensional systems in disordered lattices, Phys. Rev. A **93**, 033650 (2016).
[50] C. D'Errico and M. G. Tarallo, One-dimensional disordered bosonic systems, Atoms **9**, 112 (2021).
[51] M. Sbroscia, K. Viebahn, E. Carter, J.-C. Yu, A. Gaunt, and U. Schneider, Observing localization in a 2D quasicrystalline optical lattice, Phys. Rev. Lett. **125**, 200604 (2020).
[52] J.-C. Yu, S. Bhave, L. Reeve, B. Song, and U. Schneider, Observing the two-dimensional Bose glass in an optical quasicrystal, arXiv:2303.00737.
[53] M. Olshanii, Atomic scattering in the presence of an external confinement and a gas of impenetrable bosons, Phys. Rev. Lett. **81**, 938 (1998).
[54] M. A. Cazalilla, Bosonizing one-dimensional cold atomic gases, J. Phys. B **37**, S1 (2004).
[55] H. Yao, A. Khoudli, L. Bresque, and L. Sanchez-Palencia, Critical behavior and fractality in shallow one-dimensional quasiperiodic potentials, Phys. Rev. Lett. **123**, 070405 (2019).

[56] G. Roati, M. Zaccanti, C. D'Errico, J. Catani, M. Modugno, A. Simoni, M. Inguscio, and G. Modugno, ^{39}K Bose-Einstein condensate with tunable interactions, Phys. Rev. Lett. **99**, 010403 (2007).
[57] See Supplemental Material at http://link.aps.org/supplemental/10.1103/PhysRevLett.133.123401 for atom distribution in experiments and determination of the QMC error bars, which includes Refs. [58,59].
[58] C. D'Errico, M. Zaccanti, M. Fattori, G. Roati, M. Inguscio, G. Modugno, and A. Simoni, Feshbach resonances in ultracold ^{39}K, New J. Phys. **9**, 223 (2007).
[59] V. Dunjko, V. Lorent, and M. Olshanii, Bosons in cigar-shaped traps: Thomas-Fermi regime, Tonks-Girardeau regime, and in between, Phys. Rev. Lett. **86**, 5413 (2001).
[60] H. Yao, L. Pizzino, and T. Giamarchi, Strongly-interacting bosons at 2D-1D dimensional crossover, SciPost Phys. **15**, 050 (2023).
[61] Y. Guo, H. Yao, S. Ramanjanappa, S. Dhar, M. Horvath, L. Pizzino, T. Giamarchi, M. Landini, and H.-C. Nägerl, Observation of the 2D-1D dimensional crossover in strongly interacting ultracold bosons, Nat. Phys. **20**, 934 (2024).
[62] Y. Guo, H. Yao, S. Dhar, L. Pizzino, M. Horvath, T. Giamarchi, M. Landini, and H.-C. Nägerl, Anomalous cooling of bosons by dimensional reduction, Sci. Adv. **10**, eadk6870 (2024).
[63] L. Tanzi, S. Scaffidi Abbate, F. Cataldini, L. Gori, E. Lucioni, M. Inguscio, G. Modugno, and C. D'Errico, Velocity-dependent quantum phase slips in 1D atomic superfluids, Sci. Rep. **6**, 25965 (2016).
[64] S. Scaffidi Abbate, L. Gori, M. Inguscio, G. Modugno, and C. D'Errico, Exploring quantum phase slips in 1D bosonic systems, Eur. Phys. J. Spec. Top. **226**, 2815 (2017).
[65] C. D'Errico, S. S. Abbate, and G. Modugno, Quantum phase slips: From condensed matter to ultracold quantum gases, Phil. Trans. R. Soc. A **375**, 20160425 (2017).
[66] L. Tanzi, E. Lucioni, S. Chaudhuri, L. Gori, A. Kumar, C. D'Errico, M. Inguscio, and G. Modugno, Transport of a Bose gas in 1D disordered lattices at the fluid-insulator transition, Phys. Rev. Lett. **111**, 115301 (2013).
[67] D. M. Ceperley, Path integrals in the theory of condensed helium, Rev. Mod. Phys. **67**, 279 (1995).
[68] M. Boninsegni, N. Prokof'ev, and B. Svistunov, Worm algorithm for continuous-space path integral Monte Carlo simulations, Phys. Rev. Lett. **96**, 070601 (2006).
[69] M. Boninsegni, N. V. Prokof'ev, and B. V. Svistunov, Worm algorithm and diagrammatic Monte Carlo: A new approach to continuous-space path integral Monte Carlo simulations, Phys. Rev. E **74**, 036701 (2006).
[70] J. Vidal, D. Mouhanna, and T. Giamarchi, Interacting fermions in self-similar potentials, Phys. Rev. B **65**, 014201 (2001).
[71] C. Kollath, A. Iucci, T. Giamarchi, W. Hofstetter, and U. Schollwöck, Spectroscopy of ultracold atoms by periodic lattice modulations, Phys. Rev. Lett. **97**, 050402 (2006).
[72] G. Orso, A. Iucci, M. Cazalilla, and T. Giamarchi, Lattice modulation spectroscopy of strongly interacting bosons in disordered and quasiperiodic optical lattices, Phys. Rev. A **80**, 033625 (2009).
[73] M. Troyer, B. Ammon, and E. Heeb, in *Proceedings of the International Symposium on Computing in Object-Oriented Parallel Environments* (Springer, New York, 1998), pp. 191–198.
[74] A. Albuquerque, F. Alet, P. Corboz, P. Dayal, A. Feiguin, S. Fuchs, L. Gamper, E. Gull, S. Guertler, A. Honecker *et al.*, The ALPS project release 1.3: Open-source software for strongly correlated systems, J. Magn. Magn. Mater. **310**, 1187 (2007).
[75] B. Bauer, L. D. Carr, H. Evertz, A. Feiguin, J. Freire, S. Fuchs, L. Gamper, J. Gukelberger, E. Gull, S. Guertler *et al.*, The ALPS project release 2.0: Open source software for strongly correlated systems, J. Stat. Mech. (2011) P05001.

Supplemental Material for Mott transition for a Lieb-Liniger gas in a shallow quasiperiodic potential: Delocalization induced by disorder

Hepeng Yao,[1,*] Luca Tanzi,[2,3] Laurent Sanchez-Palencia,[4] Thierry Giamarchi,[1] Giovanni Modugno,[2,3,5] and Chiara D'Errico[6,†]

[1] *DQMP, University of Geneva, 24 Quai Ernest-Ansermet, CH-1211 Geneva, Switzerland*
[2] *Istituto Nazionale di Ottica, CNR-INO, Via Moruzzi 1, 56124 Pisa, Italy*
[3] *European Laboratory for Non-Linear Spectroscopy, Università degli Studi di Firenze, Via N. Carrara 1, 50019 Sesto Fiorentino, Italy*
[4] *CPHT, CNRS, Ecole Polytechnique, IP Paris, F-91128 Palaiseau, France*
[5] *Dipartimento di Fisica e Astronomia, Università degli Studi di Firenze, Via G. Sansone 1, 50019 Sesto Fiorentino, Italy*
[6] *Istituto per la Protezione Sostenibile delle Piante, CNR-IPSP, Strada delle Cacce 73, 10135 Torino, Italy*

(Dated: June 10, 2024)

EXPERIMENTAL PARAMETERS

Atom distribution among the tubes

The array of tubes is created starting from a BEC loaded in a 3D optical trap. A deep 2D horizontal optical lattice with spacing $d = \lambda_1/2 = 532$ nm is then adiabatically raised to a typical height of 20 recoil energies. Due to the radial trapping confinement during the loading of the 2D lattice, the 1D tubes at the center (tails) of the distribution contain more (less) particles. The exact distribution of atoms among the tubes may be estimated by assuming that the atoms are not redistributed among the tubes during the lattice loading. The distribution of the atoms in the tubes is a Thomas-Fermi, i.e.

$$N_{i,j} = N_{0,0}\left[1 - (i^2 + j^2)\frac{d^2}{R_r^2}\right]^{3/2}, \qquad \text{(S1)}$$

where m is the atomic mass, $R_r = \sqrt{2\mu/(m\omega_r^2)}$, and $\mu = \frac{\hbar\bar{\omega}}{2}(15a_{load}/\bar{\ell})^{2/5}N_T^{2/5}$. The atom number in the central tube is given by $N_{0,0} = \frac{5}{2\pi}\frac{d^2}{R_r^2}N_T$, N_T is the total atom number, ω_r ($\bar{\omega}$) is the radial (geometric mean) optical trap frequency before the loading of the tubes and $\bar{\ell} = \sqrt{\hbar/m\bar{\omega}}$. Tuning the value of the scattering length a_{load} during the loading of the 2D lattice on a Feshbach resonance [1, 2], we can slightly control μ, and thus the Thomas-Fermi distribution of the atoms in the tubes. With the parameters used in the experiment we obtain $N_{0,0} = 53 \pm 10$, whose uncertainty is due to a systematic relative uncertainty of 30% on the total atom number, and the atom distribution shown in Fig. S1a.

Atom distribution along the tubes and estimation of the mean density

Both in the horizontal direction (between tubes) and in the vertical one (along the tubes), the atom distribution is inhomogeneous. When the scattering length is tuned to the variable value a to explore the superfluid-insulator transition, the distribution inside each tube, and thus the mean density of the system, may change. On the contrary, since the tunneling time between neighboring tubes ($h/J_\perp = 0.55$ s) largely exceeds the tuning time of a (≈ 50 ms), the atom distribution between tubes should not be affected. Depending on the value of the scattering length a and the atom number, the distribution in individual tubes is expected to vary from Thomas-Fermi (weak interactions) to Tonks-Girardeau (strong interac-

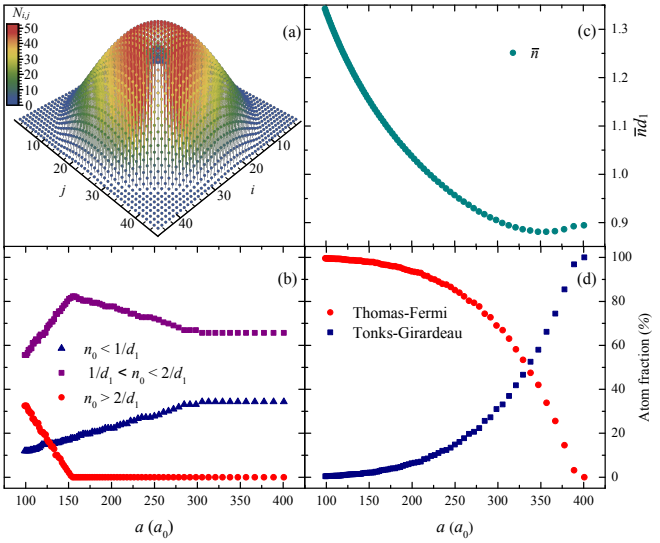

FIG. S1. (a) Distribution of the atoms in the tubes in the Thomas-Fermi approximation, with the parameters typically used in the experiment: $N_T = 35000$, $a_{load} = 226\,a_0$, $\omega_r = 2\pi \times 45$ Hz and $\bar{\omega} = 2\pi \times 49$ Hz. (b) Atom fraction in tubes with maximum density $n_0 > 2/d_1$ (red circles), $1/d_1 < n_0 < 2/d_1$ (purple squares), and $n_0 < 1/d_1$ (blue triangles), as a function of the scattering length a. (c) Mean density as a function of a. (d) Atom fraction in tubes with Thomas-Fermi (red circles), and Tonks-Girardeau (blue squares) distributions as a function of a.

tions) profiles [3]. In each tube we compare both distributions, and, as done in previous experiments [4, 5], we retain the one that maximises the central density n_0. The mean density $\bar{n}$ is then calculated by averaging overall the tubes. The value $a_{load} = 226a_0$ has been tuned to obtain a mean density $\bar{n} \approx 1/d_1$. The results of this procedure, calculated neglecting the effect of the vertical optical lattices, are shown as a function of the scattering length in Figs. S1b-d. They show the fraction of atoms in tubes with maximum density in different ranges, the mean density $\bar{n}$, and the fraction of atoms in tubes with Thomas-Fermi or Tonks-Girardeau distributions. For $V \neq 0$ the assumed distribution inside each tube is reliable only in the superfluid regime, while it fails in the Mott one. When increasing the scattering length in the region of $a > a_c$, in fact, in tubes where the Mott lobes form the density is fixed. The transport along the tubes containing one or two regions with $n = 1/d_1$ is globally suppressed, as the part of atoms reaching the Mott condition stops also the upward parts with different densities, thus driving most of the tube into an effective insulating regime. The plateau in z_c, shown in Fig. 2 (b) of the main paper, is generated by the tubes where the critical density $n = 1/d_1$ is not reached (about a 25% of atoms), as well as the downward part of tubes with MI regions (about a 10%), which keep moving also for $a > a_c$. Note that, due to the inhomogeneity of the experimental system, we estimate that about 55% of atoms are in tubes containing one or two regions with $n = 1/d_2$. However, these areas do not alter the determination of the critical point a_c, since we expect to reach the critical interaction necessary to localize fragments with $n = 1/d_1$ first. In addition, measurements with different mean densities show that the measured a_c does not substantially change with $\bar{n}$, consistently with the conjecture that the observed insulating phase is due to the Mott region with $n = 1/d_1$.

DETERMINATION OF ERRORBAR IN THE QUANTUM MONTE CARLO CALCULATIONS

When computing phase diagrams like Fig. 3 of the main paper, we need to calculate the superfluid fraction f_s and particle number N as a function of the chemical potential μ, for a fixed interaction strength g_{1D}. One detailed example is shown in Fig. S2. Here, we run simulations for the quasiperiodic systems with potential strength $V/E_r = 3.0$, coupling constant $mg_{1D}d_1/\hbar^2 = 4.0$, temperature $T = 3$ nK and system size $L = 100d_1$. We show f_s as a function of μ nearby the transition point, where the errorbars of f_s presented in the plot originates from the statistical fluctuations of QMC sampling. We set the criteria of MI phase as $f_s < 5\%$ (red dashed line) and find the transition point at $\mu_c/E_r = 0.295 \pm 0.005$. Clearly, up to our discretization $\delta\mu/E_r = 0.01$, the statistical errorbar does not influence our judgement of the critical point. Similar results are found for other potential amplitudes and interaction strengths.

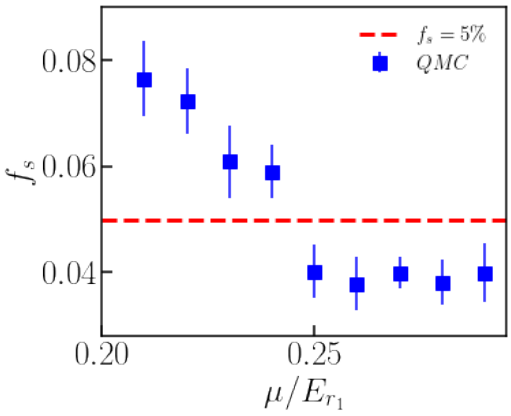

FIG. S2. One example of quantum Monte Carlo calculations for superfluid fraction f_s as a function of the chemical potential μ, for a quasiperiodic system with potential strength $V/E_r = 3.0$, coupling constant $mg_{1D}d_1/\hbar^2 = 3.5$, temperature $T = 3$ nK and system size $L = 100d_1$.

Another origin of error is the discretization in parameters scannings when computing phase diagrams like Fig. 3 in the main text. We always use $\delta\mu/E_{r1} = 0.01$ and $m\delta g_{1D}d_1/\hbar^2 = 0.5$. When computing the critical interaction values $\gamma_c = mg_c/\hbar^2 n$ in Fig. 1 of the main paper, we need to consider the contribution from both errorbars. However, we always find the second one dominants and this leads to the errorbar $\delta\gamma_c = 0.5$.

In Fig. 4 of the main paper, we also run QMC simulations for the Mott gap. Its errorbar contains not only the two stated above, but also the uncertainty of the measured 3D scattering length $a = (235 \pm 5)a_0$. This leads to the 1D coupling constant $mg_{1D}d_1/\hbar^2 = 3.97 \pm 0.11$. Combining all these errors, we find $\nu_g = (350 \pm 50)$ Hz.

* Hepeng.Yao@unige.ch
† chiara.derrico@cnr.it

[1] G. Roati, M. Zaccanti, C. D'Errico, J. Catani, M. Modugno, A. Simoni, M. Inguscio, and G. Modugno, *^{39}K Bose-Einstein condensate with tunable interactions*, **99**(1), 010403 (2007).
[2] C. D'Errico, M. Zaccanti, M. Fattori, G. Roati, M. Inguscio, G. Modugno, and A. Simoni, *Feshbach resonances in ultracold39k*, New Journal of Physics **9**(7), 223 (jul 2007).
[3] V. Dunjko, V. Lorent, and M. Olshanii, *Bosons in cigar-shaped traps: Thomas-Fermi regime, Tonks-Girardeau regime, and in between*, **86**, 5413 (2001).
[4] C. D'Errico, E. Lucioni, L. Tanzi, L. Gori, G. Roux, I. P. McCulloch, T. Giamarchi, M. Inguscio, and G. Modugno,

Observation of a disordered bosonic insulator from weak to strong interactions, **113**, 095301 (2014).

[5] L. Tanzi, E. Lucioni, S. Chaudhuri, L. Gori, A. Kumar, C. D'Errico, M. Inguscio, and G. Modugno, *Transport of a Bose gas in 1D disordered lattices at the fluid-insulator transition*, **111**, 115301 (2013).